AGU PUBLICATIONS

Radio Science

RESEARCH ARTICLE
10.1002/2015RS005856

Modeling the interference environment in the HF band

L. H. Pederick[1] and M. A. Cervera[1,2]

[1]Defence Science and Technology Group, Edinburgh, South Australia, Australia, [2]School of Physical Sciences, University of Adelaide, Adelaide, Australia

Key Points:
- We have developed a model for external interference at HF
- Can model diurnal, seasonal, and geographic variations
- Model gives results consistent with JORN spectrum monitor data

Correspondence to:
L. H. Pederick,
lenard.pederick@dsto.defence.gov.au

Citation:
Pederick, L. H., and M. A. Cervera (2016), Modeling the interference environment in the HF band, *Radio Sci.*, *51*, 82–90, doi:10.1002/2015RS005856.

Received 12 NOV 2015
Accepted 25 JAN 2016
Accepted article online 29 JAN 2016
Published online 18 FEB 2016

Abstract The performance of systems using high frequency (HF) radio waves, such as over-the-horizon radars (OTHR), can be strongly affected by external interferers at great distances (thousands of kilometers) from the systems receiver. However, the propagation of interference has complex behavior and is known to vary with location, time, season, sunspot number, and radio frequency. Understanding how the level of interference varies with all of these factors is important for the design of new systems such as next generation OTHR. By combining databases of known transmitters, ray-tracing propagation, and a model ionosphere, a model of the behavior of interference at HF has been developed.

1. Introduction

The interference environment at the receiving antenna of any system using radio waves is an important factor determining the performance of that system. For systems using high frequency (HF) radio waves, such as over-the-horizon radars (OTHR), oceanographic radars, ionospheric sounders and HF communications, this is further complicated by the ability of these waves to be refracted by the ionosphere, which allows interference to propagate over very long distances. Also, due to spatial and temporal variations in the ionosphere, the interference environment at HF has complex behavior and is known to vary with location, time, season, sunspot number, and radio frequency.

In particular, an OTHR system must be frequency agile over the whole HF band, in order to adapt to different ionospheric conditions, and its receivers must operate in the presence of large out-of-band signals (such as transmissions from broadcasters). These signals can cause several problems in an OTHR receiver, including intermodulation and cross-modulation distortion, reciprocal mixing, and blocking. Thus, knowledge of the large signal environment (i.e., the interference environment) is important in the design of any OTHR receiver.

There has been much work done on measuring and modeling the variations in spectral occupancy at HF. For several decades there has been a joint UK, Swedish, and German effort to measure and analyze the HF spectral occupancy over northern Europe, giving an empirical model for predicting the spectral occupancy [*Noble et al.*, 1995; *Pantjiaros et al.*, 1998; *Economou et al.*, 2005]. Another model was developed using data from the Jindalee facility in Central Australia [*Percival et al.*, 1997]. *Dutta and Gott* [1981] looked at modeling the propagation of interference and studying how the interference spectrum correlates between different receiving stations.

While previous efforts have provided valuable information about the interference environment and spectral occupancy within the HF band, the development and performance prediction of new radar systems requires knowledge of the directional distribution of the interference sources, as well as how they vary with the geographical location of the receiver. Following on from similar work done to model the background noise environment, we have developed SPINE: System for the Prediction of the Interference and Noise Environment. This article will only report on the interference component of SPINE; the noise component has been documented separately [*Pederick and Cervera*, 2016].

2. Interference Model Overview

The power received over a HF radio link can be expressed as [*Davies*, 1990]

$$\frac{P_r}{G_r} = \frac{P_t G_t}{L_a L_r}\left(\frac{\lambda}{4\pi R_{\text{eff}}}\right)^2, \tag{1}$$

where P_t and P_r are the transmitted and received power, G_t and G_r are the effective gains of the transmit and receive antennas, L_a represents the total ionospheric absorption loss, L_r represents the losses from ground

reflections (relevant only for multihop paths), λ is the wavelength, and R_{eff} is the effective range, taking into account the effects of ionospheric focusing.

Accurate estimates of L_a, L_r, and R_{eff} all require knowledge of the path that the radio waves take through the ionosphere, which can be calculated using ray tracing. In addition, the transmitter antenna gain G_t is a function of the departure angle (both its bearing and elevation, depending on the details of the antenna) which can be calculated by ray tracing; similarly the receive gain G_r is a function of the arrival angle.

The SPINE interference model works by determining the possible propagation paths for each known source of HF interference. This data can then be used to determine the total received power from each interference source and thus the interference environment at the receiver.

3. Transmitter Databases

The HFCC (High Frequency Coordination Committee) maintains a global database of shortwave transmissions which is published twice a year and is freely available from their website (http://www.hfcc.org). The database provides information on the location, schedule, and frequency of each transmitter, who is responsible for each transmitter, as well as various details about the transmission system, including antenna type and orientation, power output, and modulation system used.

The HFCC's database allows for a reasonable estimate of the interference sources in the HF band at any given time; however, it should be noted that it only includes shortwave broadcasters and does not include interference caused by other systems, such as oceanographic and military radars, amateur users, mobile users aboard aircraft and ships [*International Telecommunications Union*, 2012], and broadband sources (often referred to as "man-made noise") [*Spaulding et al.*, 1975] such as vehicle emission systems and power lines.

4. Propagation Model

4.1. Ray Tracing

The ray tracing to determine the propagation paths for each interference source is calculated using the PHaRLAP ray tracing software [*Cervera and Harris*, 2014]. Two-dimensional numerical ray tracing (2-D NRT) is used, including an empirical correction for magneto-ionic splitting [*Bennett et al.*, 1994]. For applications requiring greater precision, the full three-dimensional ray tracing can be used, which is more computationally intensive but allows for the effects of ionospheric tilts and more accurate calculation of magneto-ionic splitting.

Note that analytic ray tracing, which assumes a spherically symmetric ionosphere, cannot be used in SPINE due to the large distances between the interferers and the receiver, which cause large down-range variations of the ionosphere such as propagation across the equatorial anomaly or propagation from a nighttime ionosphere to a daytime ionosphere.

The electron density in the ionosphere was modeled using the International Reference Ionosphere (IRI) [*Bilitza et al.*, 2011], the de facto international standard for the climatological specification of ionospheric parameters. IRI produces monthly median values of ionospheric densities and temperatures in the nonauroral ionosphere, and can model diurnal, seasonal, solar cycle, and geographic variations. SPINE uses the most current version of IRI, IRI-2012.

Figure 1 shows the ray paths of all of the modes calculated by PHaRLAP for a 15.16 MHz transmitter at Jinhua, China, 28.07°N, 119.39°E and a receiver at Laverton, Australia, 28.33°S, 122.83°E. Visible in the plot are reflections from both the *E* and *F* layers, some magneto-ionic splitting, modes featuring different numbers of reflections (hops) from the ground as well as a chordal mode which is reflected twice by the ionosphere (at the northern and the southern anomaly regions) without reaching the ground in between the reflections.

4.2. Absorption Model

The losses due to absorption by the ionosphere are calculated using the SiMIAN absorption model [*Pederick and Cervera*, 2014]. This model integrates the absorption coefficient χ (the imaginary component of the complex refractive index) along a ray path, with the absorption coefficient calculated using the Sen-Wyller formula [*Sen and Wyller*, 1960] and the NRLMSISE-00 atmospheric model [*Picone et al.*, 2002].

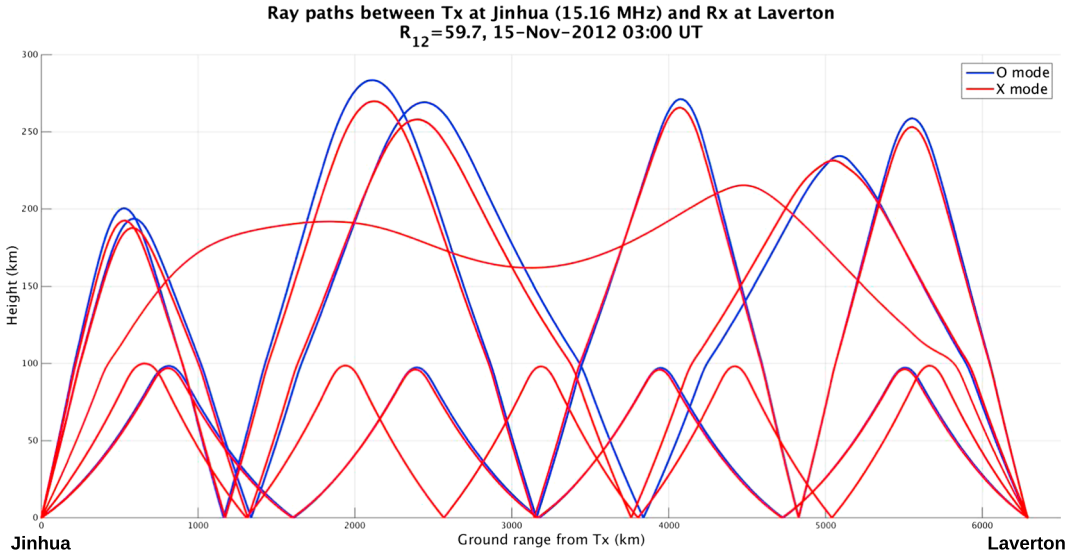

Figure 1. All of the possible modes calculated by PHaRLAP for a 15.16 MHz transmitter at Jinhua, 28.07°N, 119.39°E and a receiver at Laverton, 28.33°S, 122.83°E. *O* modes are shown in blue, *X* modes in red.

4.3. Ground Reflection Losses

As in the noise component of SPINE, the ground reflection loss L_r is given by

$$L_r = 10\log_{10}\left(\frac{|R_v|^2 + |R_h|^2}{2}\right), \tag{2}$$

where

$$R_v = \frac{n^2\sin\varphi - \left(n^2 - \cos^2\varphi\right)^{\frac{1}{2}}}{n^2\sin\varphi + \left(n^2 - \cos^2\varphi\right)^{\frac{1}{2}}}, \tag{3}$$

$$R_h = \frac{\sin\varphi - \left(n^2 - \cos^2\varphi\right)^{\frac{1}{2}}}{\sin\varphi + \left(n^2 - \cos^2\varphi\right)^{\frac{1}{2}}}, \tag{4}$$

$$n^2 = \varepsilon_r - j(1.8\times 10^4)\frac{\sigma}{f}, \tag{5}$$

ε_r is the relative dielectric constant of the Earth surface (using values of 80 for sea and 15 for land), σ is the conductivity of the surface (using 8 S/m for sea and 0.01 S/m for land), f is the propagation frequency, and φ is the elevation angle at which the ray hits the Earth's surface.

4.4. Effective Range

The effective range, R_{eff}, is a measure of how much power from a transmitter spreads out as it propagates through the ionosphere. The propagation will cause a certain power per unit area to be present at the receiver; R_{eff} is the distance at which this power would be present if there were no refraction by the ionosphere.

In SPINE, the ray tracing process involves a recursive search (in azimuth and elevation space) to find rays corresponding to each mode. The result of this search will be a set of rays (two if using 2-D NRT and three if using 3-D NRT) whose endpoints surround the receiver. The effective range can then be calculated using

$$R_{\text{eff}}^2 = \frac{A\sin\varphi}{\Delta\Omega}, \tag{6}$$

where for the 3-D NRT case, A is the area on the ground of the triangle formed by the three ray endpoints, φ is the elevation angle at the receiver, and $\Delta\Omega$ is the solid angle subtended by the three rays at the transmitter. A straightforward modification of this method is used for the 2-D NRT case [*Davies*, 1990].

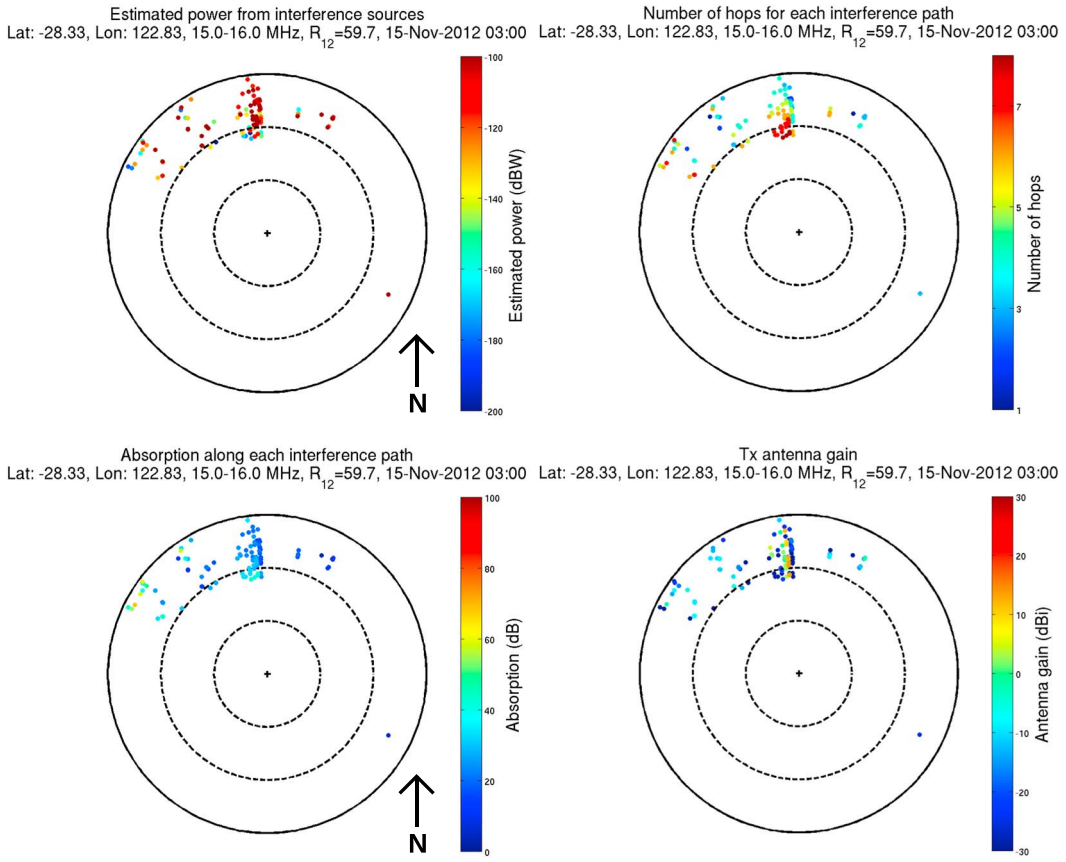

Figure 2. Interference map calculated by SPINE, for 15–16 MHz, during November 2012, late afternoon. The central point of each plot is the zenith, the outer boundary is the horizon and the two dashed circles represent 30° and 60° elevations. (clockwise from top left) Estimated power for each mode, number of hops (ionospheric reflections) for each mode, estimated transmit antenna gain, and ionospheric absorption for each mode.

5. Antenna Models

The HFCC database provides information on the type of transmit antenna used by each broadcaster, referenced to a list of antenna types maintained by the International Telecommunication Union (ITU) [*International Telecommunication Union*, 2002]. SPINE uses the formulas given by the ITU to calculate the antenna gain pattern, except for the log-periodic antennas which were modeled numerically using NEC-4. Note that the transmitter antenna gain is calculated using a simplified method and there are several effects which are not taken into account, such as variations in the electromagnetic properties of the ground and other losses within the transmission system.

6. Results

6.1. Directional Interference Map

Figure 2 shows the directional interference map output from SPINE for 15 to 16 MHz, for a receiver at Laverton (latitude 23.52°S, longitude 133.68°E) during November 2012 at 0300 UTC (11:00 local time) with a sunspot number $R_{12} = 59.7$. Figure 2 (top left) shows the estimated incoming power for each source, assuming an isotropic receive antenna. Each point represents a single mode from a transmitter. Figure 2 (top right) shows the number of hops (ionospheric reflections) for each mode, which is used for calculating ground reflection losses. Figure 2 (bottom right) shows the transmit antenna gain for each mode. Figure 2 (bottom left) shows the ionospheric absorption for each mode, as calculated by SiMIAN. Note that most of the transmitters have several possible paths (modes) to propagate to the receiver. Also, most of the transmitters appear to the northwest of the receiver, as the transmitters closest to Laverton are mostly located in southeast Asia.

Figure 3 shows an estimated interference spectrum profile, calculated from the interference map shown in Figure 2. This calculation assumes the receiver has a vertical monopole antenna and that all of the received

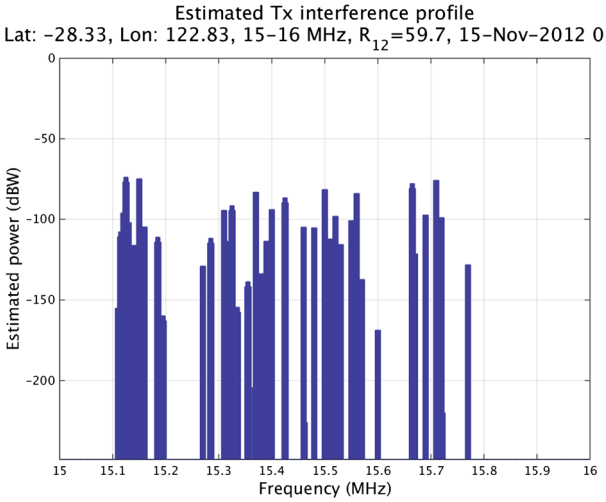

Figure 3. Estimated interference spectrum, from the interference map shown in Figure 2, assuming a vertical monopole receive antenna, 2 kHz receiver channels, and all transmitters having a bandwidth of 10 kHz.

transmissions have a bandwidth of 10 kHz with a constant power spectral density across that bandwidth. The power is estimated in 2 kHz bands.

6.2. Diurnal and Frequency Variation

Figure 4 (left) shows the total interference power expected to be received by a vertical monopole over a whole day and across all frequencies from 5 to 32 MHz, as modeled by SPINE. The results are shown for Laverton, at 28.33°S, 122.83°E, for November 2012 (R_{12} = 66.8). Figure 4 (right) shows the same results combined with the background noise calculated by the SPINE noise model, which accounts for noise originating from lightning strikes and from extraterrestrial (galactic) sources. These can be compared with Figure 5, which shows the monthly median of the background noise level observed by a spectrum monitor at Laverton. SPINE matches the diurnal and frequency variation of the interference component of the observed background noise very well. However, there are several frequency bands where interference is visible in the observed measurements but is not predicted by the model. This is due to sources of HF transmissions that are not represented in the HFCC database; for instance, interference from Citizens Band (CB) radio users is visible from 26 to 28 MHz during the daytime, and cumulative interference from other HF communications can be seen at lower frequencies during the night (from approximately 0900 to 2100 UT, below 15 MHz). Note that if we had a more complete HF transmitter database which included these transmitters, it would be simple to include them in the model.

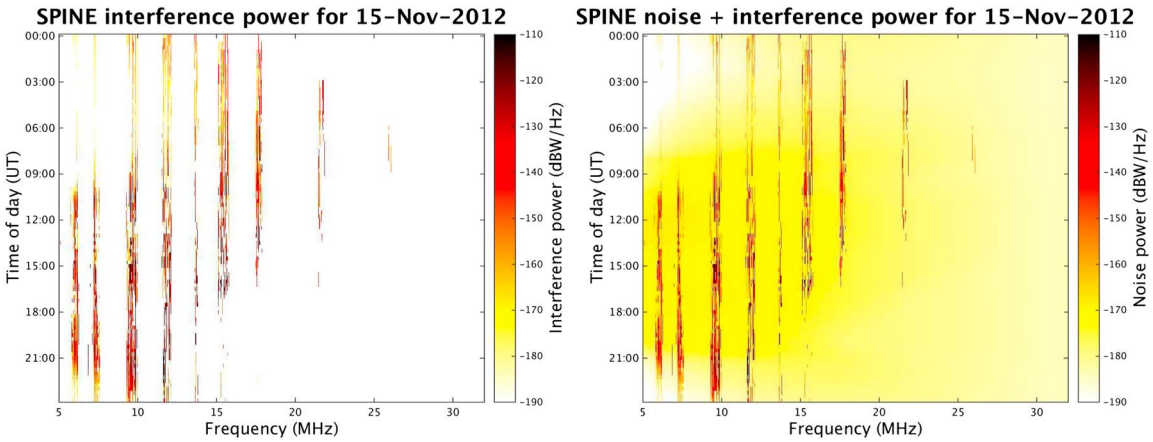

Figure 4. Estimated background noise and interference estimated by SPINE for a vertical monopole antenna at Laverton, 28.33°S, 122.83°E, for November 2012, R_{12} = 59.7. (left) Interference modeled by SPINE. (right) Sum of the interference and noise modeled by SPINE.

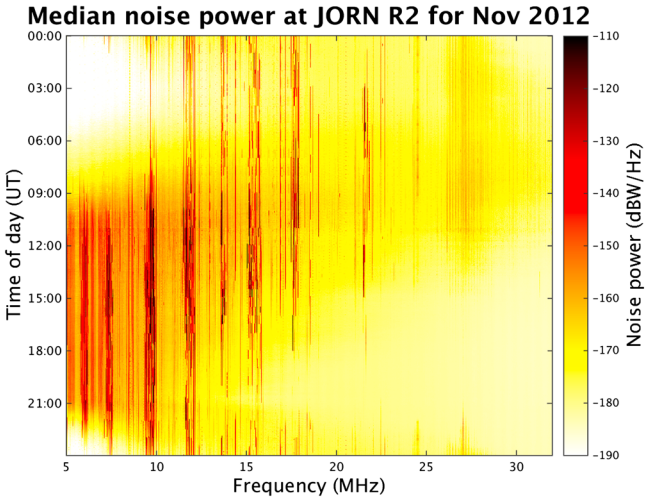

Figure 5. Monthly median background noise as seen by a monopole antenna at Laverton, 28.33°S, 122.83°E, for November 2012, $R_{12} = 59.7$.

Figure 6 shows the interference power expected to be received by a vertical monopole over a whole day, from 5 to 32 MHz, across different seasons and parts of the solar cycle. Figure 6 (left column) shows the monthly median background noise level observed by the spectrum monitor at Laverton for four representative months: January and July in 2008, when the sunspot number was low (4.2 and 2.7), and January and July in 2012, when the sunspot number was at midlevels (65.5 and 57.8). Figure 6 (right column) shows the corresponding interference level as calculated by SPINE. This figure shows that the agreement between SPINE and the Laverton noise monitor data noted in Figure 5 holds across all seasons and points in the solar cycle.

6.3. Spectral Occupancy

We also compared the model against an empirical spectral occupancy model, developed by *Economou et al.* [2005] from a series of measurements made at four different sites in northern Europe. SPINE was used to estimate the interference at Hamburg (53.54°N, 10.06°E), between the four sites where the measurements used in the Economou et al. model were taken. The congestion (spectral occupancy) in the 10 ITU frequency allocations covered by the HFCC's transmitter database (5.95, 7.10, 9.50, 11.65, 13.60, 15.10, 17.55, 18.90, 21.45, and 25.67 MHz) was then estimated. Congestion, as defined by Economou et al., is the fraction of the allocation spectral width for which the root-mean-square signal level at each step exceeds the given threshold level. We used the same bandwidth and threshold as Economou vis. 1 kHz and 1 μV/m. The congestion was calculated for local midday and midnight, for both winter and summer conditions.

Figure 7 shows the congestion calculated by SPINE compared to the congestion calculated using the model by Economou et al. The two models broadly agree, although SPINE generally predicts less congestion, again most likely due to sources of HF transmissions that are not represented in the HFCC database, as well as a contribution from man-made noise which is not modeled by SPINE. Note that SPINE cannot currently be used to estimate the spectral occupancy of other frequency allocations (outside the broadcast bands) due to the limitations of the HFCC's database.

7. Conclusion

The current paper describes a model for the interference environment at HF. This model can predict the directional distribution of interference, as well as its diurnal, seasonal, solar cycle, and geographic variation. The model agrees well with measurements made by a spectrum monitor at Laverton.

Possible future enhancements to the model include the addition of the effects of sporadic E [*Pederick*, 2014], which will improve the model's accuracy particularly at higher frequencies, improvements to the transmitter database used in the model, to include interference from other sources of HF transmissions, and further validation of the model against real measurements.

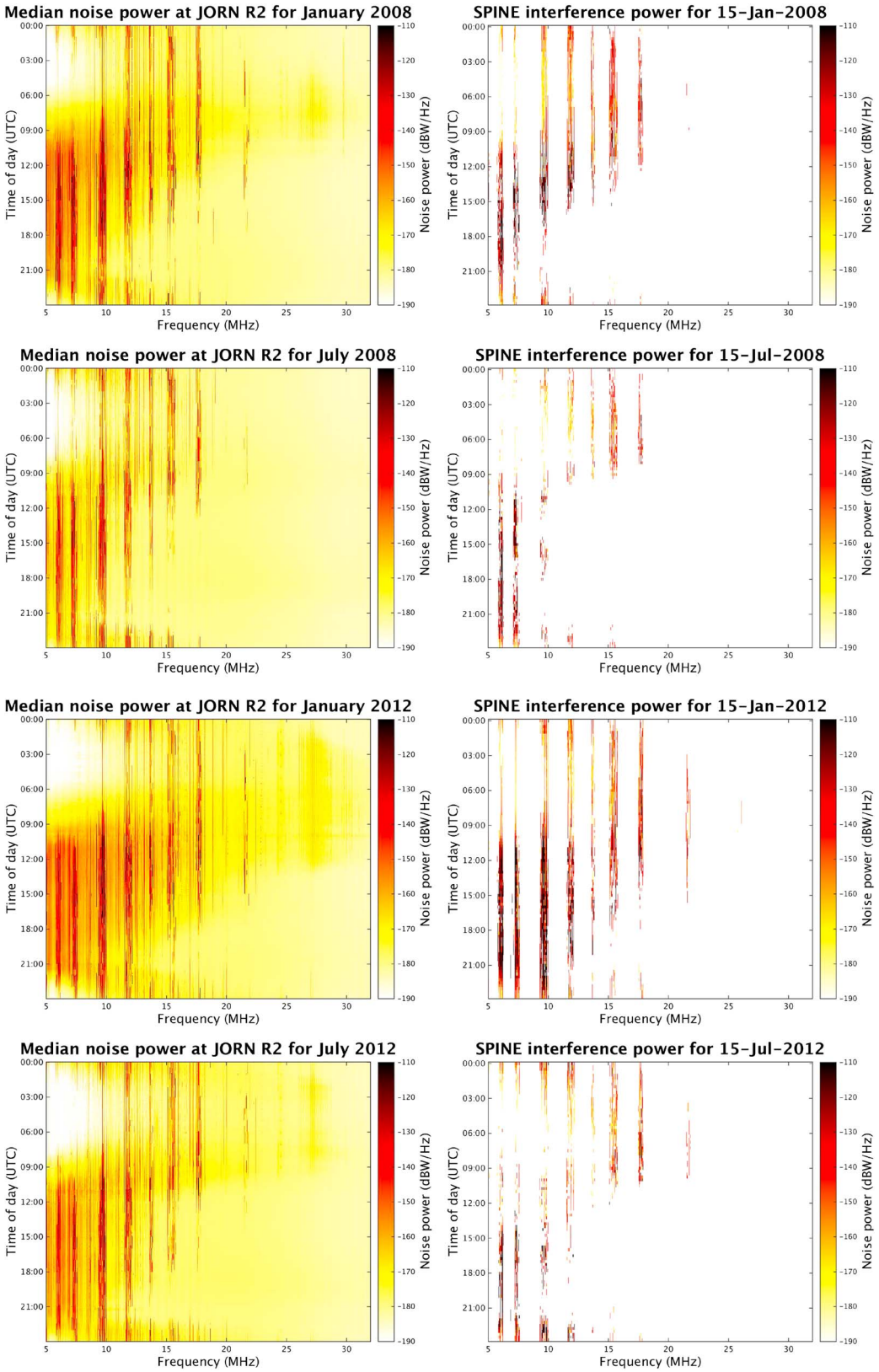

Figure 6. Comparison of background noise as seen by a monopole antenna at (left column) Laverton with the interference estimated by (right column) SPINE. The rows are, from the top, January 2008 (summer, low sunspot number), July 2008 (winter, low sunspot number), January 2012 (summer, midlevel sunspot number), and July 2012 (winter, midlevel sunspot number).

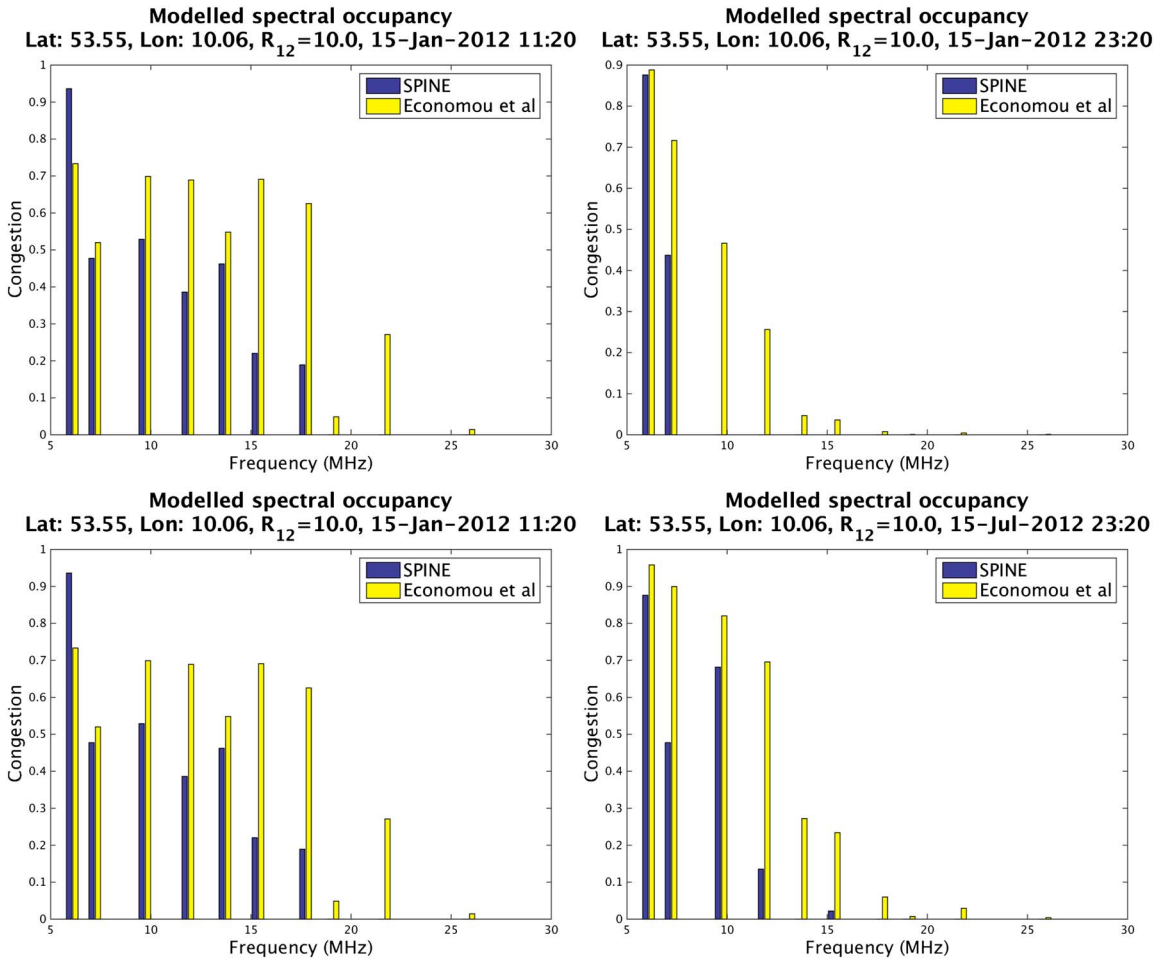

Figure 7. Comparison of the congestion estimated by SPINE and congestion estimated by a model from *Economou et al.* [2005], calculated at Hamburg. SPINE results are in dark blue. (clockwise from the top left) Daytime during winter, nighttime during winter, nighttime during summer, and daytime during summer.

Acknowledgments
The data from the JORN spectrum monitor, supporting Figure 5, are from the Australian Department of Defence. Availability of this data is limited due to national security issues.

References

Bennett, J., J. Chen, and P. Dyson (1994), Analytic calculation of the ordinary (O) and extraordinary (X) mode nose frequencies on oblique ionograms, *J. Atmos. Terr. Phys.*, *56*(5), 631–636.

Bilitza, D., L. McKinnell, B. Reinisch, and T. Fuller-Rowell (2011), The international reference ionosphere today and in the future, *J. Geod.*, *85*(12), 909–920.

Cervera, M. A., and T. J. Harris (2014), Modeling ionospheric disturbance features in quasi-vertically incident ionograms using 3-D magnetoionic ray tracing and atmospheric gravity waves, *J. Geophys. Res. Space Physics*, *119*, 431–440, doi:10.1002/2013JA019247.

Davies, K. (1990), *Ionospheric Radio*, Inst. of Eng. and Tech., London, U. K.

Dutta, S., and G. Gott (1981), Correlation of HF interference spectra with range, *IEE Proc. F*, *128*(4), 193–202.

Economou, L., H. Haralambous, C. Pantjairos, P. Green, G. Gott, P. Laycock, M. Bröms, and S. Boberg (2005), Models of HF spectral occupancy over a sunspot cycle, *IEE Proc. Commun.*, *152*(6), 980–988.

International Telecommunication Union (2002), Recommendation ITU-R BS.705-1: HF transmitting and receiving antennas characteristics and diagrams, *Tech. Rep.*, International Telecommunication Union, Geneva, Switzerland.

International Telecommunication Union (2012), *Radio Regulations*, International Telecommunication Union, Geneva, Switzerland.

Noble, A., S. Farquhar, and G. Gott (1995), Long-term measurements of occupancy in the HF band 1.5-30 MHz, in *Military Communications Conference, 1995. MILCOM'95, Conference Record*, vol. 1, pp. 113–117, IEEE, Piscataway, N. J.

Pantjiaros, C., J. Wylie, J. Brown, G. Gott, and P. Laycock (1998), Extended UK models for high frequency spectral occupancy, *IEE Proc. Commun.*, *145*, 168–174, IET.

Pederick, L. (2014), Empirical climatology of the sporadic *E* layer (ECSEL) from radio occultation measurements, paper presented at 14th Australian Space Research Conference.

Pederick, L., and M. Cervera (2014), Semiempirical model for ionospheric absorption based on the NRLMSISE-00 atmospheric model, *Radio Sci.*, *49*, 81–93, doi:10.1002/2013RS005274.

Pederick, L., and M. Cervera (2016), A directional HF noise model: Calibration and validation in the Australian region, *Radio Sci.*, *51*, doi:10.1002/2015RS005842, in press.

Percival, D., M. Kraetzl, and M. Britton (1997), A Markov model for HF spectral occupancy in central Australia, in *Seventh International Conference on HF Radio Systems and Techniques, (Conf. Publ. No. 441)*, pp. 14–18, IET, London, U. K.

Picone, J. M., A. E. Hedin, D. P. Drob, and A. C. Aikin (2002), NRLMSISE-00 empirical model of the atmosphere: Statistical comparisons and scientific issues, *J. Geophys. Res.*, *107*(A12), 1468, doi:10.1029/2002JA009430.

Sen, H. K., and A. A. Wyller (1960), On the generalization of the Appleton-Hartree magnetoionic formulas, *J. Geophys. Res.*, *65*, 3931–3950, doi:10.1029/JZ065i012p03931.

Spaulding, A., R. T. Disney, and A. Hubbard (1975), *Man-Made Radio Noise*, U.S. Dept. of Commun., Off. of Telecommun., Washington, D. C.